2013 IEEE/RSJ International Conference on
Intelligent Robots and Systems (IROS)
November 3-7, 2013. Tokyo, Japan

Stability and Efficiency of Underactuated Bipedal Walker That Generates Non-instantaneous Double-limb Support Motion

Masataka Ohshima and Fumihiko Asano

Abstract— **It was clarified that limit cycle walkers with redundant free joints generate the measurable periods of double-limb support (DLS) through numerical simulations and experiments. This paper then conducts numerical analyses to examine the effects of non-instantaneous DLS motion on the gait properties such as stability and energy efficiency. First, we divide the gait cycle into the collision and the stance phases and numerically evaluate their stability in terms of the convergence rate. Second, we analyze the stability in more detail by dividing the stance phase into the periods of DLS and single-limb support. The simulation results show that the energy efficiency monotonically worsens with the increase of the ratio of the period of DLS to the gait cycle but the convergence rate improves. Furthermore, we discuss the similarities between robot walking and human walking based on the analysis results obtained.**

I. INTRODUCTION

It is well known that limit cycle walkers smoothly walk without placing feet flat on the ground and keep walking with small energy supply. The generated gait is thus energy-efficient and high-speed, and the limit cycle consists of the stance and the collision phases. There is a tendency that the inelastic collision for stance-leg exchange is modeled on the assumption that the rear leg leaves the ground immediately after touchdown of the fore leg. The validity of this assumption has been confirmed through experimental walking of rimless wheels, compass-like walkers, and kneed walkers [1][2]. The generated gait mathematically becomes a limit cycle without containing non-instantaneous double-limb support (DLS) motion. In human walking, however, periods of non-instantaneous DLS emerge more than 10% cycle, but the effects and roles of DLS on the gait properties have not been investigated actively in the field of robotic limit cycle walking.

Recently, however, several major results have been reported. Geyer et al. discussed the similarity between human walking and limit cycle walking from the viewpoint of ground reaction forces [3]. They used the model of a planar, elastic-legged compass-like walker without having the leg mass and showed that the walker generates non-instantaneous DLS motion. Asano and Kawamoto also investigated the potentiality of emergence of non-instantaneous DLS motion through mathematical modeling and numerical simulations of more realistic spoked walker with viscoelastic-leg frames [4][5]. They showed that non-instantaneous DLS motion emerges after the instant of touchdown of the fore leg. Asano and Ohshima also numerically showed that a rimless wheel that composed on eight leg frames with active knees also generates non-instantaneous DLS motion in the case that the knee joints are kept free [6]. Furthermore, they numerically showed that a kneed bipedal walker also generates the motion by keeping the knee joints free [7].

These early works suggest that we must be careful to develop the collision model and to determine the robot's state immediately after impact if the robot has free redundant DOF. As discussed in [6][7], we can determine how the robot's state transitions during the collision phase by observing the sign of impulses acting on the fore and the rear feet. It has also been elucidated that the generated gaits including non-instantaneous DLS motion are also asymptotically stable and the convergence rate can be controlled by adjusting the system parameters. There is, however, an incomplete understanding of the qualitative properties.

Based on the observations, in this paper we conduct fundamental study on the effects of non-instantaneous DLS motion on the generated gait properties. First, we introduce a planar bipedal walker with knee joints and semicircular feet for analysis. We then perform numerical simulations and examine the inherent stability principle by dividing the walking cycle into the stance and the collision phases. We discuss the limit cycle stability from the viewpoint of the convergence rate of the state error norm. The simulation results show that the stability significantly changes with respect to the ratio of the period of DLS to the step period. Based on the results obtained, we discuss the mechanism of how elderly people fall while walking.

II. MODELING

A. Equation of Motion

This paper deals with the model of a planar biped model with active knees and semicircular feet shown in Fig. 1. This robot is composed of four links without having the inertia moment. We call the stance leg Leg 1 and swing leg Leg 2. (x, z) is the end position of Leg 1 which is identical to the attachment position of semicircular foot. The robot can exert the joint torques; u_1 and u_3 are the joint torques at the stance and the swing knees, and u_2 is the hip-joint torque.

Let $\boldsymbol{q} = \begin{bmatrix} x & z & \theta_1 & \theta_2 & \theta_3 & \theta_4 \end{bmatrix}^{\mathrm{T}}$ be the generation coordinate vector (6-DOF). The robot equation of motion then becomes

$$\boldsymbol{M}(\boldsymbol{q})\ddot{\boldsymbol{q}} + \boldsymbol{h}(\boldsymbol{q}, \dot{\boldsymbol{q}}) = \boldsymbol{S}\boldsymbol{u} + \boldsymbol{J}(\boldsymbol{q})^{\mathrm{T}}\boldsymbol{\lambda}, \quad \boldsymbol{J}(\boldsymbol{q})\dot{\boldsymbol{q}} = \boldsymbol{0}. \quad (1)$$

M. Ohshima and F. Asano are with the School of Information Science, Japan Advanced Institute of Science and Technology, 1-1 Asahidai, Nomi, Ishikawa 923-1292, Japan {ohshima_09, fasano}@jaist.ac.jp

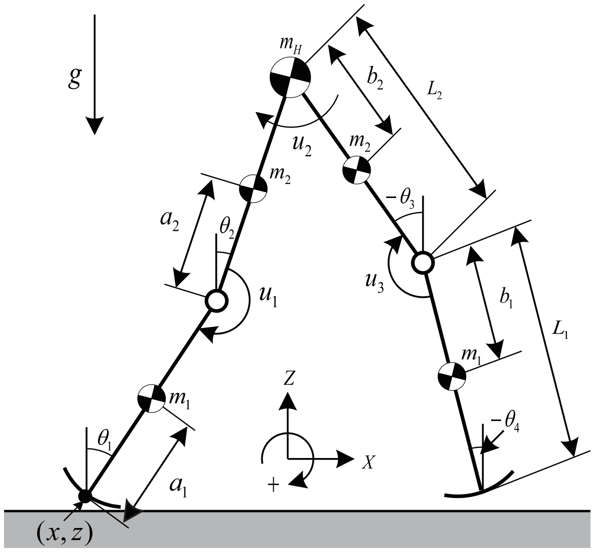

Fig. 1. Underactuated biped model with knees

Here, $\boldsymbol{Su} \in \mathbb{R}^6$ is the control input vector and is detailed as

$$\boldsymbol{Su} = \begin{bmatrix} 0 & 0 & 0 \\ 0 & 0 & 0 \\ 1 & 0 & 0 \\ -1 & 1 & 0 \\ 0 & -1 & 1 \\ 0 & 0 & -1 \end{bmatrix} \begin{bmatrix} u_1 \\ u_2 \\ u_3 \end{bmatrix}. \quad (2)$$

The second term of the right-hand side in Eq. (1) represents the holonomic constraint force vector and the elements are equal to the tangential and the normal ground reaction forces at the stance foot or at the both feet. By eliminating the undermined multiplier vector, $\boldsymbol{\lambda}$, from Eq. (1), we obtain

$$\begin{aligned} \boldsymbol{M}(\boldsymbol{q})\ddot{\boldsymbol{q}} &= \boldsymbol{Y}(\boldsymbol{q})(\boldsymbol{Su} - \boldsymbol{h}(\boldsymbol{q}, \dot{\boldsymbol{q}})) \\ &\quad - \boldsymbol{J}(\boldsymbol{q})^{\mathrm{T}} \boldsymbol{X}(\boldsymbol{q})^{-1} \dot{\boldsymbol{J}}(\boldsymbol{q}, \dot{\boldsymbol{q}})\dot{\boldsymbol{q}}, \end{aligned} \quad (3)$$

where $\boldsymbol{X}(\boldsymbol{q}) := \boldsymbol{J}(\boldsymbol{q})\boldsymbol{M}(\boldsymbol{q})^{-1}\boldsymbol{J}(\boldsymbol{q})^{\mathrm{T}}$ and

$$\boldsymbol{Y}(\boldsymbol{q}) := \boldsymbol{I}_6 - \boldsymbol{J}(\boldsymbol{q})^{\mathrm{T}}\boldsymbol{X}^{-1}\boldsymbol{J}(\boldsymbol{q})\boldsymbol{M}(\boldsymbol{q})^{-1}.$$

The robot has two or four holonomic constraints in accordance with the number of the support legs.

B. Phase Sequence

The robot generates walking gaits by actuating the three joints according to the method described later. The generated gait includes both non-instantaneous DLS and single-limb support (SLS) phases, and is divided into the following three phases according to the contact conditions.

- Collision phase (Touch down of the swing leg)
- Stance phase 1: Period of DLS (2-DOF)
- Stance phase 2: Period of SLS (4-DOF)

The Jacobian matrix, $\boldsymbol{J}(\boldsymbol{q})$, in Eq. (1) is exchanged in accordance with the holonomic constraint conditions.

1) Period of DLS: In this period, the following two conditions hold.

(C1) The sole of Leg 1 contacts the floor without slipping. Rolling constraint is guaranteed.

(C2) The sole of Leg 2 contacts the floor without slipping. Rolling constraint is guaranteed.

$\boldsymbol{J}(\boldsymbol{q})$ is then derived by summarizing four equations representing these conditions. In this period, the 6-DOF system has four constraint conditions and the motion therefore becomes 2-DOF and the holonomic constraint forces can be divided into

$$\boldsymbol{J}_{\mathrm{DLS}}(\boldsymbol{q})^{\mathrm{T}}\boldsymbol{\lambda} = \sum_{j=1}^{4} \boldsymbol{J}_j(\boldsymbol{q})^{\mathrm{T}}\lambda_j, \quad (4)$$

where $\boldsymbol{J}_j(\boldsymbol{q}) \in \mathbb{R}^{1\times 6}$ is the (j)th row vector of $\boldsymbol{J}_{\mathrm{DLS}}(\boldsymbol{q}) \in \mathbb{R}^{4\times 6}$ and $\lambda_j \in \mathbb{R}$ is the (j)th component of $\boldsymbol{\lambda} \in \mathbb{R}^4$. The Jacobian vectors $\boldsymbol{J}_1(\boldsymbol{q})$ and $\boldsymbol{J}_2(\boldsymbol{q})$ corresponds to the constraint condition (C1), whereas $\boldsymbol{J}_3$ and $\boldsymbol{J}_4$ corresponds to (C2). The vertical ground reaction force acting on the contact point of Leg 1 with the ground is represented by λ_2, and that of Leg 2 is represented by λ_4. Both of them must be positive during DLS motion and we can detect the instant that Leg 2 leaves the ground by observing the sign of λ_4.

2) Period of SLS: In this period, only the condition (C1) holds. The Jacobian matrix therefore becomes

$$\boldsymbol{J}_{\mathrm{SLS}}(\boldsymbol{q}) = \begin{bmatrix} \boldsymbol{J}_1(\boldsymbol{q}) \\ \boldsymbol{J}_2(\boldsymbol{q}) \end{bmatrix}. \quad (5)$$

C. Collision Equation

After having calculated the velocity immediately after the impact without changing the swing leg for the stance leg, we take the way to change velocity of Leg 1 and Leg 2. Let $\boldsymbol{q}^-$ be the velocity immediately before impact and $\boldsymbol{q}^+$ be that immediately after impact, the collision equation becomes

$$\boldsymbol{M}(\boldsymbol{q})\dot{\boldsymbol{q}}^+ = \boldsymbol{M}(\boldsymbol{q})\dot{\boldsymbol{q}}^- + \boldsymbol{J}_I(\boldsymbol{q})^{\mathrm{T}}\boldsymbol{\lambda}_I, \quad \boldsymbol{J}_I(\boldsymbol{q})\dot{\boldsymbol{q}}^+ = \boldsymbol{0}. \quad (6)$$

Here, we do not consider the stance-leg exchange and thus $\boldsymbol{q} = \boldsymbol{q}^{\pm}$. We exchange the positional coordinates after computing the post-impact velocities. By solving the above equations, the velocity vector immediately after impact can be derived as

$$\dot{\boldsymbol{q}}^+ = \left(\boldsymbol{I}_6 - \boldsymbol{M}(\boldsymbol{q})^{-1}\boldsymbol{J}_I(\boldsymbol{q})^{\mathrm{T}}\boldsymbol{X}_I(\boldsymbol{q})^{-1}\boldsymbol{J}_I(\boldsymbol{q})\right)\dot{\boldsymbol{q}}^-, \quad (7)$$

where $\boldsymbol{X}_I(\boldsymbol{q}) := \boldsymbol{J}_I(\boldsymbol{q})\boldsymbol{M}(\boldsymbol{q})^{-1}\boldsymbol{J}_I(\boldsymbol{q})^{\mathrm{T}}$ and the Jacobian matrix at impact, $\boldsymbol{J}_I(\boldsymbol{q})$, is exchanged in accordance with the following algorithm.

(A1) We set $\boldsymbol{J}_I(\boldsymbol{q}) = \boldsymbol{J}_{\mathrm{DLS}}(\boldsymbol{q})$ in Eq. (6) and compute $\boldsymbol{\lambda}_I \in \mathbb{R}^4$.

(A2) Divide $\boldsymbol{\lambda}_I$ into $\boldsymbol{\lambda}_I = \begin{bmatrix} \lambda_{I1} & \lambda_{I2} & \lambda_{I3} & \lambda_{I4} \end{bmatrix}^{\mathrm{T}}$. $\lambda_{I2} \geq 0$ and $\lambda_{I4} \geq 0$ must hold to transition to DLS. It is obvious, however, that $\lambda_{I2} \geq 0$ always holds. Therefore we should check the sign of λ_{I4} only.

(A3) If $\lambda_{I4} < 0$, DLS motion does not emerge. We then compute $\dot{\boldsymbol{q}}^+$ by setting $\boldsymbol{J}_I(\boldsymbol{q}) = \boldsymbol{J}_{\mathrm{SLS}}(\boldsymbol{q})$.

(A4) If $\lambda_{I4} \geq 0$, the motion then transitions to DLS and we compute $\dot{\boldsymbol{q}}^+$ by setting $\boldsymbol{J}_I(\boldsymbol{q}) = \boldsymbol{J}_{\mathrm{DLS}}(\boldsymbol{q})$.

D. Detection of takeoff of Leg2

Leg 2 begins to leave the ground at the instant that the sign of λ_4 in Eq. (4) continuously changes from positive to negative. The problem is, however, that the vertical (normal) ground reaction force immediately after impact, λ_4^+, does not become positive even if λ_{I4} is positive in the case that collision occurs while keeping the knee-joint actuation. In the case that the robot mechanically locks all the joints or does not have redundant joints, the sign of the vertical (normal) velocity at rear foot immediately after impact is equal to that of $-\lambda_{I4}$ [8][9]. In other words, the rear foot always leaves the ground immediately after impact if $\lambda_{I4} > 0$. In the presence of redundant free joints [6][7], however, the same is not true and we must be careful to determine the post-impact situation.

We then take the following computational procedure based on the sign of λ_4^+.

(B1) If $\lambda_{I4} \geq 0$, the motion is determined to transition to DLS. The collision equation are then specified as

$$\boldsymbol{M}(\boldsymbol{q}^+)\ddot{\boldsymbol{q}}^+ + \boldsymbol{h}(\boldsymbol{q}^+, \dot{\boldsymbol{q}}^+) = \boldsymbol{S}\boldsymbol{u} + \boldsymbol{J}_{\mathrm{DLS}}(\boldsymbol{q}^+)^{\mathrm{T}}\boldsymbol{\lambda}^+, \quad (8)$$

$$\boldsymbol{J}_{\mathrm{DLS}}(\boldsymbol{q}^+)\dot{\boldsymbol{q}}^+ = \boldsymbol{0}_{4\times 1}. \quad (9)$$

Note that, however, $\boldsymbol{q}^+$ in the above equations is the positional vector after exchanging the coordinates.

(B2) Divide $\boldsymbol{\lambda}^+$ in Eq. (8) into $\boldsymbol{\lambda}^+ = \begin{bmatrix} \lambda_1^+ & \lambda_2^+ & \lambda_3^+ & \lambda_4^+ \end{bmatrix}^{\mathrm{T}}$. If $\lambda_2^+ \geq 0$ and $\lambda_4^+ \geq 0$, then we take $\ddot{\boldsymbol{q}}^+$ obtained in (B1) and continue the numerical integral.

(B3) If $\lambda_2^+ \geq 0$ and $\lambda_4^+ < 0$, unilateral constraint condition is not satisfied and the motion should transition to SLS. We then break $\ddot{\boldsymbol{q}}^+$ obtained in (B1) and solve the following equations for $\dot{\boldsymbol{q}}^+$.

$$\boldsymbol{M}(\boldsymbol{q}^+)\ddot{\boldsymbol{q}}^+ + \boldsymbol{h}(\boldsymbol{q}^+, \dot{\boldsymbol{q}}^+) = \boldsymbol{S}\boldsymbol{u} + \boldsymbol{J}_{\mathrm{SLS}}(\boldsymbol{q}^+)^{\mathrm{T}}\boldsymbol{\lambda}^+ \quad (10)$$

$$\boldsymbol{J}_{\mathrm{SLS}}(\boldsymbol{q}^+)\dot{\boldsymbol{q}}^+ = \boldsymbol{0}_{2\times 1} \quad (11)$$

We take the newly-calculated $\ddot{\boldsymbol{q}}^+$ from Eq. (10) as the proper initial acceleration vector and begin the numerical integral.

In the case of (B3), the rear foot leaves the ground immediately after impact. The generated DLS motion is therefore instantaneous although the collision equation used $\boldsymbol{J}_{\mathrm{DLS}}(\boldsymbol{q}^+)$.

III. LEVEL GAIT GENERATION

A. Control Phase I

Let $t = 0$ [s] be the instant of touchdown of the swing leg. In this phase, we do not exert all the joint torques. Non-instantaneous DLS motion then continues.

B. Control Phase II

The control phase II starts at $t = T_1(> 0)$ [s]. In this control phase, we set the knee-joint torques, u_1 and u_3, to constant values determined in advance. This control is continued for T_2 [s]. We concurrently control the hip-joint to follow a desired-time trajectory. Let us divide the control input vector into

$$\boldsymbol{S}\boldsymbol{u} = \begin{bmatrix} 0 & 0 \\ 0 & 0 \\ 1 & 0 \\ -1 & 0 \\ 0 & 1 \\ 0 & -1 \end{bmatrix} \begin{bmatrix} u_1 \\ u_3 \end{bmatrix} + \begin{bmatrix} 0 \\ 0 \\ 0 \\ 1 \\ -1 \\ 0 \end{bmatrix} u_2 = \boldsymbol{S}_{13}\boldsymbol{u}_{13} + \boldsymbol{S}_2 u_2. \quad (12)$$

Let the relative hip-joint angle, $\theta_H := \theta_2 - \theta_3$, be the control output in this phase. Its second-order derivative with respect to time becomes

$$\ddot{\theta}_H = A_{\mathrm{II}}(\boldsymbol{q})u_2 + B_{\mathrm{II}}(\boldsymbol{q}, \dot{\boldsymbol{q}}), \quad (13)$$

where $A_{\mathrm{II}}(\boldsymbol{q}) := \boldsymbol{S}_2^{\mathrm{T}}\boldsymbol{M}(\boldsymbol{q})^{-1}\boldsymbol{Y}(\boldsymbol{q})\boldsymbol{S}_2$ and

$$\begin{aligned} B_{\mathrm{II}}(\boldsymbol{q}, \dot{\boldsymbol{q}}) := & \ \boldsymbol{S}_2^{\mathrm{T}}\boldsymbol{M}(\boldsymbol{q})^{-1}\boldsymbol{Y}(\boldsymbol{q})(\boldsymbol{S}_{13}\boldsymbol{u}_{13} - \boldsymbol{h}(\boldsymbol{q}, \dot{\boldsymbol{q}})) \\ & -\boldsymbol{S}_2^{\mathrm{T}}\boldsymbol{M}(\boldsymbol{q})^{-1}\boldsymbol{J}(\boldsymbol{q})^{\mathrm{T}}\boldsymbol{X}(\boldsymbol{q})^{-1}\dot{\boldsymbol{J}}(\boldsymbol{q}, \dot{\boldsymbol{q}})\dot{\boldsymbol{q}}. \end{aligned}$$

The control input for achieving $\ddot{\theta}_H = v_2$ can be determined as $u_2 = A_{\mathrm{II}}(\boldsymbol{q})^{-1}(v_2 - B_{\mathrm{II}}(\boldsymbol{q}, \dot{\boldsymbol{q}}))$ where

$$v_2 = \ddot{\theta}_{H\mathrm{d}}(t) + K_D(\dot{\theta}_{H\mathrm{d}}(t) - \dot{\theta}_H) + K_P(\theta_{H\mathrm{d}}(t) - \theta_H). \quad (14)$$

Here, K_P and K_D are PD gains and are positive constants. The desired-time trajectories for hip-joint, $\theta_{H\mathrm{d}}(t)$, is given as a five-order function of time that satisfies the boundary conditions of $\theta_{H\mathrm{d}}(0^+) = \alpha'$, $\theta_{H\mathrm{d}}(T_{\mathrm{set}}) = \alpha$, and $\dot{\theta}_{H\mathrm{d}}(0^+) = \dot{\theta}_{H\mathrm{d}}(T_{\mathrm{set}}) = \ddot{\theta}_{H\mathrm{d}}(0^+) = \ddot{\theta}_{H\mathrm{d}}(T_{\mathrm{set}}) = 0$. Here, α' [rad] is the hip-joint angle at the beginning time of the control phase II, and T_{set} is the desired settling time for the output following control. As described later, Leg 2 begins to leave the ground after exerting the knee-joint torques during this phase.

C. Control Phase III

At $t = T_2(> T_1)$ [s], we start an output PD control for the relative knee-joint angles to straighten them. They are settled to the desired terminal values. In this phase, we choose the control output vector as

$$\boldsymbol{y} := \begin{bmatrix} \theta_1 - \theta_2 \\ \theta_2 - \theta_3 \\ \theta_3 - \theta_4 \end{bmatrix} = \boldsymbol{S}^{\mathrm{T}}\boldsymbol{q}. \quad (15)$$

The second-order derivative with respect time becomes

$$\ddot{\boldsymbol{y}} = \boldsymbol{S}^{\mathrm{T}}\ddot{\boldsymbol{q}} = \boldsymbol{A}_{\mathrm{III}}(q)\boldsymbol{u} - \boldsymbol{B}_{\mathrm{III}}(\boldsymbol{q}, \dot{\boldsymbol{q}}), \quad (16)$$

where $\boldsymbol{A}_{\mathrm{III}}(\boldsymbol{q}) := \boldsymbol{S}^{\mathrm{T}}\boldsymbol{M}(\boldsymbol{q})^{-1}\boldsymbol{y}(\boldsymbol{q})\boldsymbol{S}$ and

$$\begin{aligned} \boldsymbol{B}_{\mathrm{III}}(\boldsymbol{q}, \dot{\boldsymbol{q}}) := & \ \boldsymbol{S}^{\mathrm{T}}\boldsymbol{M}(\boldsymbol{q})^{-1}(\boldsymbol{y}(\boldsymbol{q})\boldsymbol{h}(\boldsymbol{q}, \dot{\boldsymbol{q}}) \\ & +\boldsymbol{J}(\boldsymbol{q})^{\mathrm{T}}\boldsymbol{X}(\boldsymbol{q})^{-1}\dot{\boldsymbol{J}}(\boldsymbol{q}, \dot{\boldsymbol{q}})\dot{\boldsymbol{q}}). \end{aligned}$$

The control input for achieving $\ddot{\boldsymbol{y}} = \boldsymbol{v}$ can be determined as

$$\boldsymbol{u} = \boldsymbol{A}_{\mathrm{III}}(\boldsymbol{q})^{-1}\left(\boldsymbol{v} + \boldsymbol{B}_{\mathrm{III}}(\boldsymbol{q}, \dot{\boldsymbol{q}})\right), \quad (17)$$

and each element of the vector $\boldsymbol{v} = \begin{bmatrix} v_1 & v_2 & v_3 \end{bmatrix}^{\mathrm{T}}$ can be determined as $v_j = -K_D\dot{y}_j + K_P(y_{j\mathrm{d}} - y_j)$ ($j = 1$ or 3), and v_2 is the same as Eq. (14). The relative knee-joint angles, y_1 and y_3, are then controlled to the desired terminal values,

$y_{1\mathrm{d}} = \beta$ and $y_{3\mathrm{d}} = -\beta$ [rad], whereas the relative hip-joint angle, θ_H, is controlled and maintained to the desired terminal value, α [rad], where $t \geq T_{\mathrm{set}}$.

IV. STABILITY ANALYSIS

A. Preliminaries

Let us define approximate transition functions of the state error for the stance and the collision phases. In limit cycle walkers that fall down as a 1-DOF rigid body immediately before impact, we can consider only the error of the angular velocity at impact because the positional errors are always zero due to the constraint on impact posture [10][11]. By linearizing the equation of motion, we can analytically derive the transition function of the state error for the stance phase as

$$\Delta\dot{\theta}^-_{1(i+1)} = \bar{Q}\Delta\dot{\theta}^+_{1(i)}. \tag{18}$$

This is available if the walker keeps locking all the joints during the collision phases. To derive $\bar{Q}$, we must apply some linear approximations [11]. The error terms higher than second order neglected in the derivation, however, are not sufficiently small and there is a considerable difference between the values of $\bar{Q}$ and of the real walking system [12].

The walker in this paper does not mechanically lock the joints during the collision phases, so we should introduce more generalized transition function. For example, the following function can be considered as a candidate.

$$\hat{Q}_{(i)} := \frac{\left\| \Delta\dot{\boldsymbol{\theta}}^-_{(i+1)} \right\|}{\left\| \Delta\dot{\boldsymbol{\theta}}^+_{(i)} \right\|} \tag{19}$$

We assumed, however, that the error norm of the angular position is sufficiently smaller than that of the angular velocity, i.e. $\left\| \Delta\dot{\boldsymbol{\theta}}^\pm_{(i)} \right\| \gg \left\| \Delta\boldsymbol{\theta}^\pm_{(i)} \right\|$ holds. Note that $\hat{Q}_{(i)}$ is the transition equation not for the state error but for the state error norm of the (i)th step. Therefore $\hat{Q}_{(i)}$ is always positive and is not useful for evaluating the convergence property, speed mode or totter mode.

We further consider to compute the mean value of $\hat{Q}_{(i)}$ on the assumptions that $\hat{Q}_{(i)}$ shows little change. Define $\hat{Q}$ as the mean value of $\hat{Q}_{(i)}$ for the first five steps, that is,

$$\hat{Q} := \frac{1}{5}\sum_{i=0}^{4} \hat{Q}_{(i)}. \tag{20}$$

The transition function of the state error for the collision phase of the (i)th step is also defined as

$$\hat{R}_{(i)} := \frac{\left\| \Delta\dot{\boldsymbol{\theta}}^+_{(i)} \right\|}{\left\| \Delta\dot{\boldsymbol{\theta}}^-_{(i)} \right\|}. \tag{21}$$

We then compute the mean value in the same way as

$$\hat{R} := \frac{1}{5}\sum_{i=0}^{4} \hat{R}_{(i)}. \tag{22}$$

B. Evolution of State Error in Typical Walking Gait

Fig. 2 shows the evolution of the state error norm in level dynamic walking where $T_1 = 0.05$, $T_2 = 0.15$ [s] and $\beta = 0$ [rad]. The physical parameters were chosen as listed in Table I. The PD gains were also chosen as $K_D = 60$ and $K_P = 900$. We can see that the stance phases are stable but the collision phases are unstable and that the overall generated gait is asymptotically stable. Specifically, the values of the transition functions were $\hat{Q} = 0.480$, $\hat{R} = 1.250$, and $\hat{Q}\hat{R} = 0.60$. The convergence property is classified into the speed mode because of $0 < \hat{Q}\hat{R} < 1$. In a passive compass gait, the stance phase is unstable but the collision phase is stable [13]. Interestingly, however, the roles of each phase are inverted in this level gait with redundancy. As one of the authors showed, in an underactuated bipedal gait with constraint on impact posture, the stance phase is relatively higher than the collision phase in stability [11]. This is achieved by the effect of the trajectory tracking (output following) control during the stance phases. The same is true in a level gait containing non-instantaneous DLS motion.

C. Roles of SLS and DLS

Next, we analyze the roles of SLS and DLS motions in detail. Let us divide the transition function $\hat{Q}$ at instant of transition from DLS to SLS, that is,

$$\hat{Q}_{\mathrm{DLS}(i)} := \frac{\left\| \Delta\dot{\boldsymbol{\theta}}^{\mathrm{trans}}_{(i)} \right\|}{\left\| \Delta\dot{\boldsymbol{\theta}}^+_{(i)} \right\|}, \tag{23}$$

$$\hat{Q}_{\mathrm{SLS}(i)} := \frac{\left\| \Delta\dot{\boldsymbol{\theta}}^-_{(i+1)} \right\|}{\left\| \Delta\dot{\boldsymbol{\theta}}^{\mathrm{trans}}_{(i)} \right\|}. \tag{24}$$

Here, $\Delta\dot{\boldsymbol{\theta}}^{\mathrm{trans}}_i \in \mathbb{R}^4$ is the error vector of the angular velocity at instant of transition from DLS to SLS. These functions satisfy the relation $\hat{Q}_{(i)} = \hat{Q}_{\mathrm{DLS}(i)}\hat{Q}_{\mathrm{SLS}(i)}$.

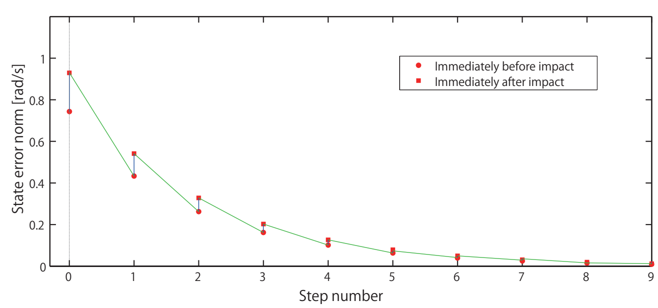

Fig. 2. Evolution of state error norm with respect to step number

TABLE I
PARAMETER SETTINGS

m_H	10.0	kg	a_1,a_2	0.3	m
m_1	1.0	kg	b_1,b_2	0.2	m
m_2	10.0	kg	L_1	0.5	m
α	0.6	rad	L_2	0.5	m
R	0.5	m	u_1	10	N·m
T_{set}	0.4	s	u_2	40	N·m

We can change the ratio of the period of DLS to the gait cycle by adjusting the control timing, T_1 and T_2, while keeping T_{set} constant. Fig. 3 shows the evolutions of the state error norms with respect to step number for three values of DLS ratio without dividing the stance phases. Whereas Fig. 4 shows that dividing the stance phases. Here, $T_1 = 0.01$ [s] and $T_2 = 0.08$ [s] for DLS of 12%, $T_1 = 0.05$ [s] and $T_2 = 0.15$ [s] for that of 22%, and $T_1 = 0.10$ [s] and $T_2 = 0.22$ [s] for that of 30%. We can see that the stance phases are stable but the collision phases are unstable in all cases and that the convergence rate becomes faster with the increase of DLS ratio. To perform numerical comparison, we also compute the mean values of $\hat{Q}_{\mathrm{DLS}(i)}$ and $\hat{Q}_{\mathrm{SLS}(i)}$ as follows.

$$\hat{Q}_{\mathrm{DLS}} := \frac{1}{5}\sum_{i=0}^{4}\hat{Q}_{\mathrm{DLS}(i)} \tag{25}$$

$$\hat{Q}_{\mathrm{SLS}} := \frac{1}{5}\sum_{i=0}^{4}\hat{Q}_{\mathrm{SLS}(i)} \tag{26}$$

Table II lists the values of the transition functions corresponding to the three generated gaits in Figs. 3 and 4. From the values of the DLS ratio and the $\hat{Q}$, we can see that the convergence rate monotonically improves with the increase of the DLS ratio. The Poincaré return map, $\hat{Q}\hat{R}$, therefore monotonically decreases with the increase of the DLS ratio because $\hat{R}$ is constant. Both the values of $\hat{Q}_{\mathrm{DLS}}$ and $\hat{Q}_{\mathrm{SLS}}$ also monotonically decrease with the increase of the DLS ratio and $\hat{Q}_{\mathrm{DLS}} > \hat{Q}_{\mathrm{SLS}}$. The high convergence rate in the SLS might be achieved mainly by the effect of the tracking control to the desired-time trajectories as in the case of the compass gait [11].

In the following, we analyze the gait properties in more detail by using various criteria and discuss the relation between the convergence speed and the gait efficiency.

The walking speed, V [m/s], is defined as

$$V := \frac{\Delta X_g}{T}, \tag{27}$$

where T [s] is the step period and ΔX_g [m] is the step length which is determined as

$$\Delta X_g = R\alpha + 2(L_1 + L_2 - R)\sin\frac{\alpha}{2}. \tag{28}$$

The cadence (gait frequency) which represents the number of steps per minute is defined as

$$\mathrm{Cadence} := \frac{V}{\Delta X_g} = \frac{1}{T}. \tag{29}$$

The cost of transport is evaluated in terms of specific resistance (SR) defined as

$$\mathrm{SR} := \frac{p}{MgV}, \tag{30}$$

where p [J/s] is the average input power given by

$$p := \frac{1}{T}\int_0^T \sum_{i=1}^{3}\left|u_i\left(\dot{\theta}_i - \dot{\theta}_{i+1}\right)\right| \mathrm{d}t. \tag{31}$$

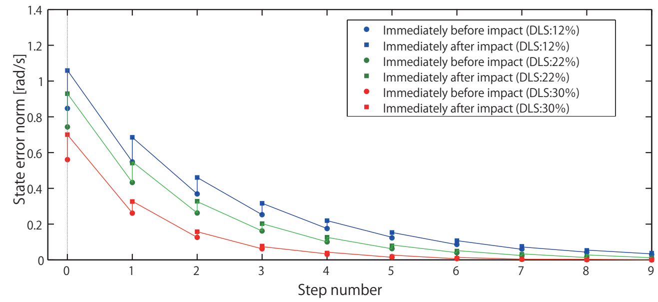

Fig. 3. Evolutions of state error norms with respect to step number for three values of DLS ratio

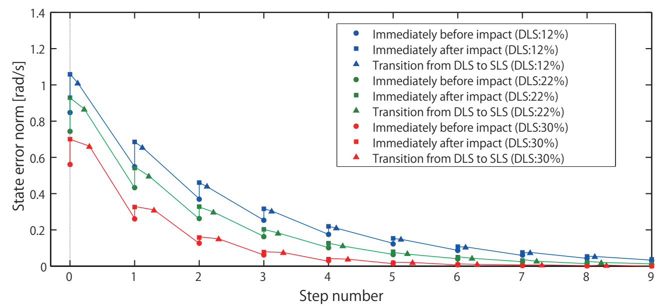

Fig. 4. Evolutions of state error norm with respect to step number for three values of DLS ratio

TABLE II

VALUES OF TRANSITION FUNCTIONS IN CHANGE OF DLS RATIO

DLS [%]	$\hat{Q}$ [-]	$\hat{Q}_{\mathrm{DLS}}$ [-]	$\hat{Q}_{\mathrm{SLS}}$ [-]	$\hat{Q}\hat{R}$ [-]
12.3	0.540	0.952	0.581	0.675
22.1	0.483	0.946	0.507	0.560
30.3	0.367	0.939	0.413	0.462

TABLE III

GAIT EFFICIENCIES WITH RESPECT TO DLS RATIO

DLS [%]	v [m/s]	Cadence [step/min]	p [J/s]	SR [-]
12	0.92	93.6	46.1	0.16
22	0.90	91.5	90.3	0.33
30	0.81	83.2	150.0	0.58

Table III lists changes in the criteria in the three generated gaits of Figs. 3 and 4 with respect to the DLS ratio. It is clear that the increase of the DLS ratio decreases the walking speed and the energy efficiency. Considering the results in Table II and III, we must conclude that there is a trade-off between the convergence speed and the gait efficiencies. To clarify these properties in more detail, we conducted numerical simulations. Fig. 5 shows (a) the step period and the walking speed and (b) the SR with respect to the DLS ratio. From Fig. 5 (a), we can see that the step period monotonically increases with the DLS ratio whereas the walking speed monotonically decreases with it. As a natural consequence, as shown in Fig. 5 (b), the SR monotonically increases with it.

Asano and Kawamoto showed that an active viscoelastic-

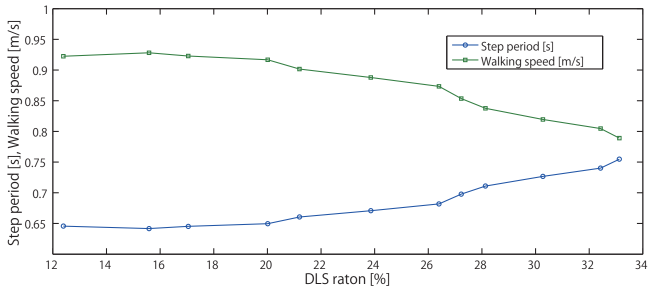

(a) Step period and walking speed

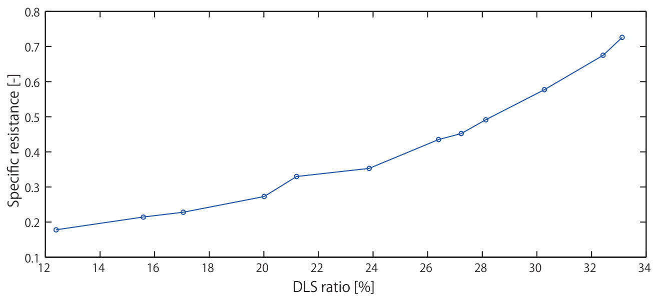

(b) Specific resistance

Fig. 5. Gait efficiencies with respect to rate of DLS period

legged rimless (VRW) wheel generates non-instantaneous DLS motion through numerical simulations and experiments [4]. They also found that the adaptability to irregular terrain of the VRW is higher than the rigid-legged one although the generated walking speed is slower [5]. This suggests that non-instantaneous DLS motion also creates a trade-off between the adaptability and the gait efficiency. These properties are summed up that non-instantaneous DLS motion tends to improve the gait robustness in terms of return speed but to worsen the gait efficiencies. The authors consider that non-instantaneous DLS motion plays a role of placing feet flat on the ground and this effectively resets or reduces the state error.

The trade-off between the DLS ratio and the gait efficiencies is true for human walking. The change tendency that the walking speed and cadence monotonically decrease with the increase of the DLS ratio can be seen in human aging [14][15]. Some control laws or mechanisms that shorten the period of DLS would tend to improve the gait efficiency in robot walking as well as human walking. Locking the knee joints at the instant of landing of the fore leg would also inhibit destabilization of the collision phase and avoid fall caused by knee buckling in elderly people walking.

V. CONCLUSION AND FUTURE WORK

In this paper, we discussed the roles of non-instantaneous DLS motion in stable gait generation of an underactuated bipedal walker. Through numerical simulations, we clarified the following qualitative characteristics.

- In a kneed walker that generates non-instantaneous DLS motion by output following control, the stance phase is stable but the collision phase is unstable.
- The convergence rate of the state error monotonically increases as the ratio of the period of DLS to the gait cycle increases.
- Both the SLS and DLS motions are stable and the convergence rate in the former is faster than that in the latter.
- The walking speed and cadence monotonically decrease with the increase of the DLS ratio and this change tendency is the same as human walking.

We must consider, however, our analysis results are just some numerical examples. More detailed analysis, especially mathematical explanations, are necessary to elucidate general case. Nevertheless, we believe that the results obtained in this paper give important basis for understanding human walking.

ACKNOWLEDGMENT

This research was partially supported by a Grant-in-Aid for Scientific Research, (C) No. 24560542, provided by the Japan Society for the Promotion of Science (JSPS).

REFERENCES

[1] T. McGeer, "Passive dynamic walking," *Int. J. of Robotics Research*, Vol. 9, No. 2, pp. 62–82, 1990.
[2] T. McGeer, "Passive walking with knees," *Proc. of the IEEE Int. Conf. on Robotics and Automation*, Vol. 3, pp. 1640–1645, 1990.
[3] H. Geyer, A. Seyfarth and R. Blickhan, "Compliant leg behaviour explains basic dynamics of walking and running," *Proc. of the Royal Society B*, Vol. 273, No. 1603, pp. 2861–2867, 2006.
[4] F. Asano and J. Kawamoto, "Passive dynamic walking of viscoelastic-legged rimless wheel," *Proc. of the IEEE Int. Conf. on Robotics and Automation*, pp. 2331–2336, 2012.
[5] J. Kawamoto and F. Asano, "Active viscoelastic-legged rimless wheel with upper body and its adaptability to irregular terrain," *Proc. of the IEEE/RSJ Int. Conf. on Intelligent Robots and Systems*, pp. 157–162, 2012.
[6] F. Asano and M. Ohshima, "Emergence of measurable period of double-limb support in limit cycle walking with knees," *Proc of the IEEE Int. Conf. on Control Applications*, pp. 1045–1050, 2012.
[7] M. Ohshima and F. Asano, "Underactuated bipedal walking with knees that generates measurable period of double-limb support," *Proc. of the IEEE Int. Conf. on Robotics and Automation*, pp. 5643–5648, 2013.
[8] J.-M. Bourgeot, C. Canudas-de-Wit and B. Brogliato, "Impact shaping for double support walk: from the rocking block to the biped robot," *Proc. of the 8th Int. Conf. on Climbing and Walking Robots and the Support Technologies for Mobile Robots*, pp. 509–516, 2005.
[9] J. M. Font-Llagunes and J. Kövecses, "Dynamics and energetics of a class of bipedal walking systems," *Mechanism and Machine Theory*, Vol. 44, Iss. 11, pp. 1999–2019, 2009.
[10] J. W. Grizzle, G. Abba and F. Plestan, "Asymptotically stable walking for biped robots: Analysis via systems with impulse effects," *IEEE Trans. on Automatic Control*, Vol. 46, No. 1, pp. 51–64, 2001.
[11] F. Asano, "Stability analysis of underactuated bipedal gait using linearized model," *Proc. of the 11th IEEE-RAS Int. Conf. on Humanoid Robots*, pp. 282–287, 2011.
[12] F. Asano, "Analytical solution to transition function of state error in 1-DOF semi-passive dynamic walking," *Proc. of the IEEE/RSJ Int. Conf. on Intelligent Robots and Systems*, 2013. (to appear)
[13] F. Asano, "Stability analysis of passive compass gait using linearized model," *Proc. of the IEEE Int. Conf. on Robotics and Automation*, pp. 557–562, 2011.
[14] J. C. Wall, D. B. Hogan, G. I. Turnbull and R. A. Fox, "The kinematics of idiopathic gait disorder: A comparison with healthy young and elderly females," *Scand. J. Med.*, Vol. 23, pp. 159–164, 1991.
[15] Y. Barak, R. C. Wagenaar and K. G. Holt, "Gait characteristics of elderly people with a history of falls: a dynamic approach," *Physical Therapy*, Vol. 86, pp. 1501–1510, 2006.